Ultrafast energy transfer from rigid, branched side-chains into a conjugated, alternating copolymer

Graham B. Griffin, Pamela M. Lundin, Brian S. Rolczynski, Alexander Linkin, Ryan D. McGillicuddy, Zhenan Bao, and Gregory S. Engel

Citation: The Journal of Chemical Physics **140**, 034903 (2014); doi: 10.1063/1.4855156
View online: http://dx.doi.org/10.1063/1.4855156
View Table of Contents: http://scitation.aip.org/content/aip/journal/jcp/140/3?ver=pdfcov
Published by the AIP Publishing

Ultrafast energy transfer from rigid, branched side-chains into a conjugated, alternating copolymer

Graham B. Griffin,[1,a)] Pamela M. Lundin,[2,3,a)] Brian S. Rolczynski,[1] Alexander Linkin,[1] Ryan D. McGillicuddy,[1] Zhenan Bao,[2] and Gregory S. Engel[1,b)]
[1]*Department of Chemistry, The James Franck Institute, Institute for Biophysical Dynamics, The University of Chicago, Chicago, Illinois 60637, USA*
[2]*Department of Chemical Engineering, Stanford University, Stauffer III, 381 North-South Mall, Stanford, California 94305, USA*
[3]*A. R. Smith Department of Chemistry, Appalachian State University, 417 CAP Building, 525 Rivers Street, Boone, North Carolina 28608, USA*

(Received 29 September 2013; accepted 9 December 2013; published online 21 January 2014)

We present the synthesis and characterization of a benzodithiophene/thiophene alternating copolymer decorated with rigid, singly branched pendant side chains. We characterize exciton migration and recombination dynamics in these molecules in tetrahydrofuran solution, using a combination of static and time-resolved spectroscopies. As control experiments, we also measure electronic relaxation dynamics in isolated molecular analogues of both the side chain and polymer moieties. We employ semi-empirical and time-dependent density functional theory calculations to show that photoexcitation of the decorated copolymer using 395 nm laser pulses results in excited states primarily localized on the pendant side chains. We use ultrafast transient absorption spectroscopy to show that excitations are transferred to the polymer backbone faster than the instrumental response function, ~250 fs. © *2014 AIP Publishing LLC*. [http://dx.doi.org/10.1063/1.4855156]

INTRODUCTION

In organic photovoltaic devices (OPVs), photoexcitation creates excitons in an electron donor material that subsequently diffuse until they recombine or achieve charge separation, typically by encountering an electron acceptor.[1,2] If the exciton reaches an acceptor, the potential energy difference between the donor and acceptor excited states can drive electron transfer across the interface, in competition with the attractive Coulombic potential between the geminate electron and hole.[3] Charge carrier diffusion is also important in emerging OPV materials that support exciton dissociation in the donor material itself.[4–18] In either case, minimizing recombination losses is an important factor in OPV device design. Directed exciton flow in these types of materials can reduce recombination losses, relative to the losses seen in purely diffusive systems, through optimization of hole or electron transfer to their respective charge-collecting components.

Controlling intramolecular excitation migration in conjugated polymers may benefit many emergent technologies such as organic light-emitting diodes,[19–24] organic field-effect transistors,[25–28] organic spintronics,[23,29,30] and OPVs.[31–38] Such organic devices offer attractive properties such as light weight, reel-to-reel processability,[39] Earth-abundant constituent materials, relatively low manufacturing cost,[33] synthetic tunability,[40,41] and mechanical flexibility.[33,42] Controlled, predictable excitation migration may also aid optimization of power conversion efficiency in OPV devices.[43]

In this work, we demonstrate directed intramolecular excited population migration from light-absorbing conjugated side chains into a conjugated polymer by exploiting a downhill energy gradient. In Fig. 1, we highlight the overall molecular design architecture employed both structurally and energetically. Conjugated polymer photophysics have previously been manipulated by changing the monomer units within the conjugated backbone, or affixing electron-donating or accepting pendant moieties to the backbone.[38,41,44–48] Such pendant moieties shift the energy levels of the conjugated chromophores to which they are attached. In contrast, we exploit intramolecular energy transfer in conjugated polymers with optically active side chains. This approach differs from previous designs that have created energy flow from the polymer into the side chains.[49,50] We seek to use the side chains as covalently linked, light harvesting antennae. Similar strategies have achieved light harvesting by antenna moieties using dye molecules hydrogen-bonded to conjugated polymers[51] or macrocycles encircling the polymer backbone.[52] By employing downhill energy transfer to drive antenna-like function in the side chains, we necessarily impart an energy loss that lowers the energy collection efficiency of the system for OPV applications. However, the goal of the present design is to use antennae to harvest high energy photons that would otherwise not be collected. Imparting an energy loss to drive this mechanism still results in improved photon collection, relative to an identical, antenna-less polymer.

Dendrimers, a family of highly branched macromolecules, have been investigated as light-harvesting antennae, typically coupled to small molecule energy sinks.[53–58] The singly branched side chain (BSC) we employ in this study is a simple first generation dendrimer, also

a)G. B. Griffin and P. M. Lundin contributed equally to this work.
b)Author to whom correspondence should be addressed. Electronic mail: gsengel@uchicago.edu.

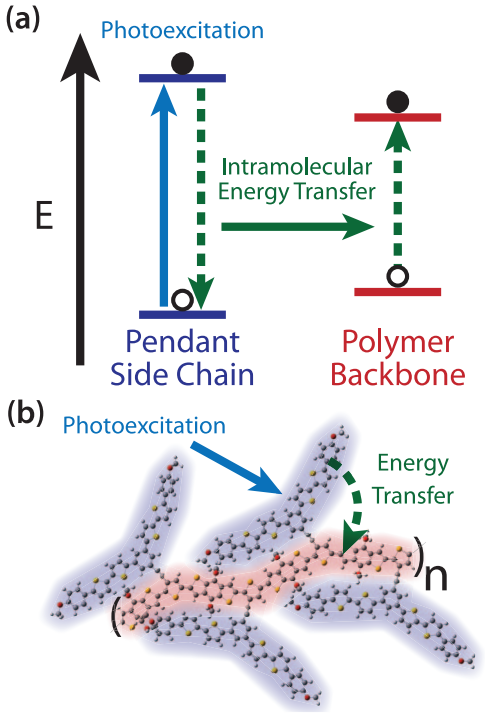

FIG. 1. Intramolecular exciton migration: (a) Photoexcitation (cyan) of optically active, singly branched side chains (blue) leads to intramolecular energy transfer (green) into the conjugated copolymer backbone (red). In this diagram, holes are shown as unfilled circles and excited electrons are shown as filled circles. Intramolecular energy transfer moves excitation energy but not charge carriers. After energy transfer the side chain is in its ground state and the polymer backbone is excited. The optical gaps of the side chain and polymer moieties can be determined from the absorption spectra presented below, and are represented accurately. The electron binding energies are currently unknown, meaning that the relative depth of side chain and polymer energy levels may vary from what is shown here. (b) Molecular design of the decorated copolymer, DCP. Singly branched side chains, highlighted in blue, are attached to an alternating copolymer (BDT/thiophene) backbone, highlighted in red. Our experimental and computational results will show that photoexcitation (cyan) of the side chains is followed by rapid intramolecular energy transfer (green) into the polymer.

called a dendron. Higher orders of branching in the side chain moiety are required to create a true dendronized polymer. By coupling an optically active dendron side chain to a conjugated polymer, we investigate a new topology for design of a light harvesting antenna system including a polymeric excitation sink. Dendronized, conjugated polymers have been previously characterized using a combination of electrochemical and spectroscopic techniques,[59–66] employing optically inactive dendrimer side chains that shield the polymer core from its surrounding environment. The present study is distinct from this previous work in that the dendron side chains employed here are both optically active and bound to the polymer backbone with a rigid linker. Rigid dendrimers have only been used in a few previous molecular designs,[67,68] in which the dendrimers were employed to manipulate the three-dimensional morphology of dendronized polymers.

In this study, we describe the design and synthesis of a decorated copolymer (DCP) macromolecule; we then use a combination of spectroscopy and electronic structure calculations to characterize its intramolecular electronic relaxation dynamics. We compare our results to characterization of representative analogues of DCP's components: the BSCs and the conjugated, alternating copolymer (PLMR). Using a combination of density functional theory and semi-empirical calculations, we assign the absorption spectrum of each material. We find that absorption bands of DCP correspond either to excitations primarily localized on its dendron side chain or primarily on the polymer backbone components. We use a combination of static and time dependent spectroscopies to investigate relaxation dynamics subsequent to excitation for the three components. We validate our molecular design by showing that the pendant side chain groups act as antennae and funnel the excitations into the conjugated polymer backbone. The DCP molecule is designed as a model system in which to demonstrate the principle that covalently bound side chains can act as light harvesting antennae. Optimization of the antenna/polymer system to minimize energy losses during the energy transfer process is left as a subject for future work.

EXPERIMENTAL METHODS

Synthesis

The synthesis of DCP is outlined in Fig. 2 (see supplementary material).[69] We chose a macromonomer approach over a graft-to approach.[59] The macromonomer approach permits incorporation of the side chain at a regular position along the polymer backbone, and preliminary attempts at a graft-to approach revealed problems with alkynyl crosslinking. The single side chain branch **1** was prepared by Stille coupling of 1-bromo-4-(2-ethylhexyl)oxy)benzene with 5-trimethylstannyl-2,2′-bithiophene, using an admixture of Pd_2dba_3 and tri-*tert*-butylphosphonium tetrafluoroborate in the presence of potassium fluoride in DMF. Following sequential lithiation and stannylation of **1**, it was then coupled to 1,3-dibromo-5-(triisopropylsilylethynyl)benzene using similar Stille coupling conditions, yielding **2**. Deprotection of **2** using tetrabutylammonium fluoride enabled Sonogashira coupling to 2,5-dibromo-3-iodothiophene to afford the macromonomer **3**. Copolymerization of **3** with the benzodithiophene monomer **4** using a Stille polycondensation under microwave conditions[70] yielded our model dendronized polymer, DCP. The M_w and M_n values were found to be 92.4 kg/mol and 54.6 kg/mol, respectively, using gel-permeation chromatography. These values indicate a high degree of polymerization, which suggests that despite the steric bulk of the macromonomer, the polymerization was not inhibited.

To compare the spectroscopic characteristics of DCP with those of its isolated components, model structures for the side chain moiety and the conjugated alternating copolymer, shown in Fig. 3, were used as control samples. BSC contains a chlorine atom meta to the two branches of the dendron, and was prepared by Stille couplings similar to those described above for the synthesis of DCP (see supplementary material).[69] PLMR contains a trialkylsilyl protecting group in place of the dendron at the 3-alkynyl position of the thiophene comonomer. It was prepared by a Stille polycondensation of a 3-alkynyl-2,5-dibromothiophene with the BDT comonomer.[69]

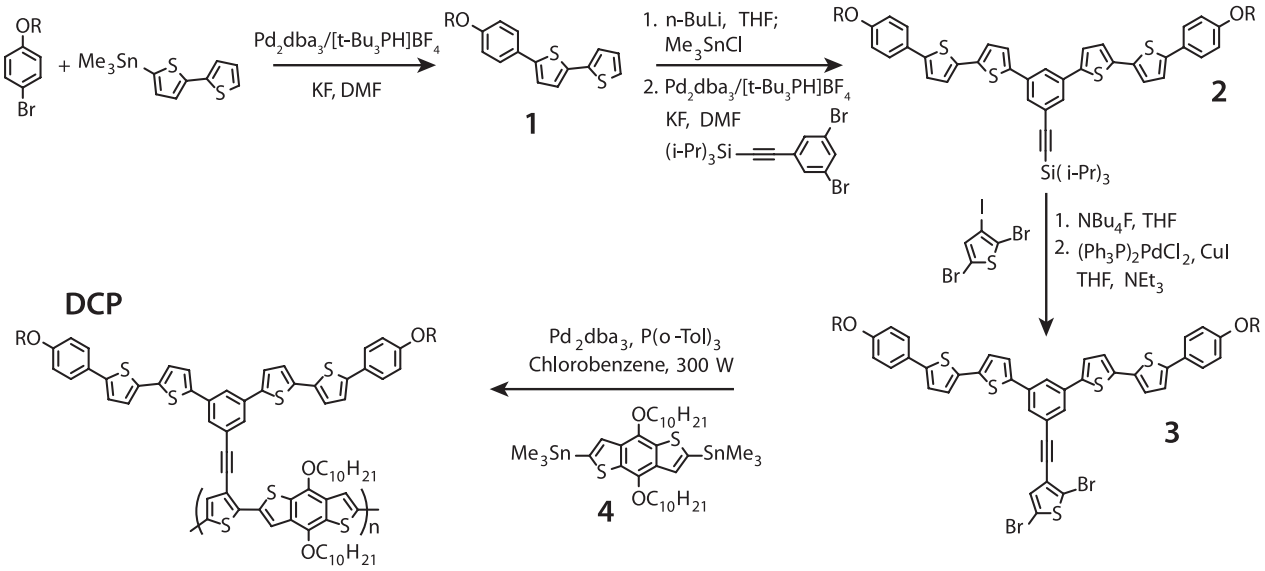

FIG. 2. Synthetic strategy: Outline of the synthetic strategy yielding the decorated copolymer macromolecule DCP. "R" represents 2-ethylhexyl.

Absorption and fluorescence spectra

We measure the room-temperature absorption spectra of BSC, PLMR, and DCP in tetrahydrofuran (THF) solution using a Unico SQ-2802 single-beam scanning UV/Visible Spectrophotometer. We measure room temperature fluorescence emission spectra and fluorescence excitation spectra of BSC, PLMR, and DCP with a Horiba Fluorolog-3 fluorometer, with excitation at 394 nm (see supplementary material).[69]

Transient absorption

Pump-probe transient absorption experiments were performed at the Center for Nanoscale Materials at Argonne National Laboratory, using HELIOS and EOS transient absorption spectrometers from Ultrafast Systems. Each material was prepared in THF solution, with concentration set such that the absorption through the 0.2 cm sample cell was A $\approx$ 0.2 at 395 nm. The samples were continuously stirred during the experiments. For all experiments, pump and probe laser beams were co-focused into a $\sim$250 μm spot in the sample. The pump pulse power was attenuated to avoid damage to the sample ($\sim$25 nJ/pulse at 0.833 kHz) using a neutral density filter.

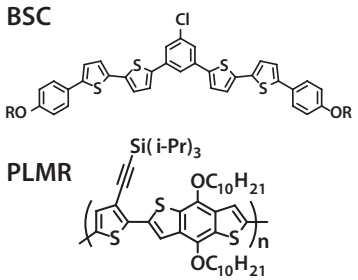

FIG. 3. Side chain and polymer analogues: The chemical structure of the model compounds for the branched side chain (BSC, top) and the conjugated, alternating copolymer (PLMR, bottom).

To investigate ultrafast dynamics, the output of a regeneratively amplified Ti:sapphire laser (Spectra-Physics Tsunami oscillator and Spitfire-Pro amplifier) is used to generate both pump and probe pulses. Pump pulses at 395 nm and 515 nm are produced using an optical parametric amplifier (TOPAS-C from Spectra-Physics), pumped with the Ti:sapphire output beam, and subsequent frequency conversion. A broadband probe beam is generated by focusing the Ti:sapphire output beam into a sapphire plate. The time-delay between the arrival of pump and probe laser pulses is generated by a computer-controlled delay stage. At each time-delay between pump and probe laser pulses, a transmission spectrum of the probe beam is measured both in the presence and the absence of the pump, and the difference of the two spectra is the transient absorption spectrum for that time delay. Time delays to be sampled were chosen to detect dynamics on all accessible timescales, from hundreds of femtoseconds to a few nanoseconds. The instrument response function is measured in a separate experiment, and wavelength dependent time delays are chirp-corrected. The instrument response function itself has a width of $\sim$250 fs FWHM for each probe wavelength. Scattered light is measured separately and subtracted prior to analysis.

To measure microsecond-regime dynamics, we use a distinct but related experimental approach. Pump beams are generated in the same way, while the probe beam is generated by focusing the output of an independent Nd:YAG laser into a photonic-crystal fiber. Transmission spectra of the probe beam are recorded in the presence and absence of the pump pulse, generating transient absorption spectra in the same fashion as the ultrafast experiments. Pump probe delay for each laser shot is measured using a digital analyzer and the recorded spectra are binned by time-delay in increments as small as 100 ps, building up the transient absorption data as a histogram. Experiments reported in this study monitor the first 0.6 μs of time delays, with binning in 5 ns increments. Chirp correction is unnecessary for these spectra because the smallest time-delay (5 ns) is three orders of magnitude larger than

the maximum chirp to be corrected (~2 ps.) Scattered light is again measured separately and subtracted prior to analysis.

Computational methods

We perform structural optimizations and single-point excited state energy calculations for representative analogs of DCP, BSC, and PLMR, using density functional theory and semi-empirical methods.[69,71] All calculations were performed on The University of Chicago Department of Chemistry's Plutonium Cluster, an 18 node, 64-bit linux system from PSSC Labs. In accordance with prior computational studies,[72] we use tetramer fragments (in which each monomer of the fragment constitutes a thiophene-benzodithiophene pair) to represent PLMR and DCP, providing a balance between accuracy and computation time. For DCP calculations, the unconjugated alkyl side chains on both the pendant side chains and the polymer backbone are reduced to methyl groups to reduce computational time. Calculations of BSC and PLMR analogs are performed using the full alkyl side chains. For BSC calculations, the meta-substituted Cl atom in the central phenyl ring (see Fig. 3) was replaced with a hydrogen atom to reduce computational cost while preserving meta-substitution about the phenyl core. For PLMR calculations, the trialkylsilyl protecting group at the linking site (see Fig. 3) is replaced with a hydrogen atom to reduce computational time. We optimize the structure of each molecule at the B3LYP/6-31G* level,[73] then perform single point time-dependent density functional theory (TDDFT)/6-31G*[74] and ZINDO/S[75] calculations to characterize each molecule's low-lying optical transitions. All calculations were performed in the gas phase. The primary purpose of the calculations is to demonstrate trends in optical excitations of these molecules and to determine localization of excitations, rather than to compute chemically accurate transition energies or electron binding energies. Because DCP and PLMR are large polymers, we must use reduced model systems such as representative tetramers to keep our computational costs reasonable. We perform our calculations in the gas phase rather than adding a solvent model to further simplify the calculation. We do not expect that addition of a solvent will substantially affect the structure of the calculated molecular orbitals (MOs) or the trends in the calculated optical excitations.

RESULTS AND DISCUSSION

Design strategy and synthesis

We designed DCP as a model molecule to demonstrate controlled energy transfer from branched, rigid, optically active side chains into a conjugated, alternating copolymer. We created strong coupling between monomer units within the polymer backbone to establish strongly mixed MOs and excitations delocalized across several monomer units in the polymer backbone. In contrast, we engineered weak coupling between the singly branched side chain moieties and the polymer, permitting excitations in DCP to be primarily localized on either the side chain or the polymer (see supplementary material).[69] We established the desired weak coupling through meta-substitution about the benzene core of the side chain. A 5,5′-diphenyl-2,2-bithiophene moiety was chosen for the basis of our singly branched dendron side chains, due to strong absorption at 400 nm.[76] The emission profile of the side chain was used to guide the choice of constituent monomers for the conjugated, alternating copolymer backbone. Planar BDT monomers, in combination with a thiophene bearing a linker to the side chain, produced a copolymer showing strong absorbance in the emission region of the side chain. An alkyne linker was chosen due to its short length and rigidity, maximizing energy transfer yield while promoting consistent spacing between the side chain and polymer chromophores.

The BSC analogue

In this section, we present results characterizing electronic relaxation dynamics in a representative analog of the singly branched pendant side chain groups, BSC, in dilute THF solution. Fig. 4 shows the B3LYP-optimized structure of BSC and the experimental linear absorption and fluorescence spectra. The linear absorption spectrum of BSC shows a strong, roughly symmetric absorption feature centered at 394 nm. Excitation at 394 nm results in a flat-topped emission feature peaking at 475 nm. The flat-topped shape likely results from a vibronic progression. The B3LYP-optimized structure of the BSC-analogue exhibits out-of-plane twisting around the thiophene groups, a well-known feature of polythiophenes with attached substituent groups.[77] Excited state TDDFT and ZINDO calculations based on this structure both yield a single strong optical transition to the lowest energy excited state (oscillator strength f = 2.6163, 2.2229, respectively). We assign the 394 nm feature in the absorption spectrum to this excitation, which is predicted to consist primarily of the HOMO-1 to LUMO (TDDFT 41%, ZINDO 45%) and HOMO to LUMO + 1 (41%, 44%) transitions (see supplementary material).[69] Both transitions involve electron density bunching toward the center of the molecule, rearrangement of the double-bond structure from aromatic to quinoidal form, and increased nodal character, typical of a $\pi-\pi^*$ transition.[69,79]

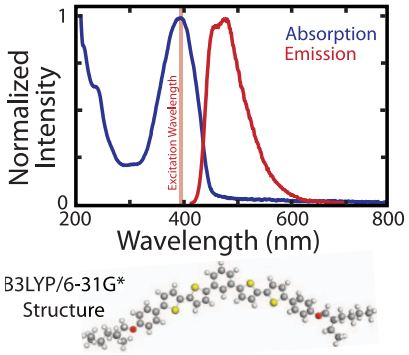

FIG. 4. Absorption and emission spectra of BSC and optimized molecular structure: (Top) absorption (blue) and fluorescence emission (red, 394 nm excitation) spectra for BSC in THF solution. (bottom) B3LYP-optimized structure of a BSC-analogue. Atoms are color coded (white = H, grey = C, red = O, yellow = S).

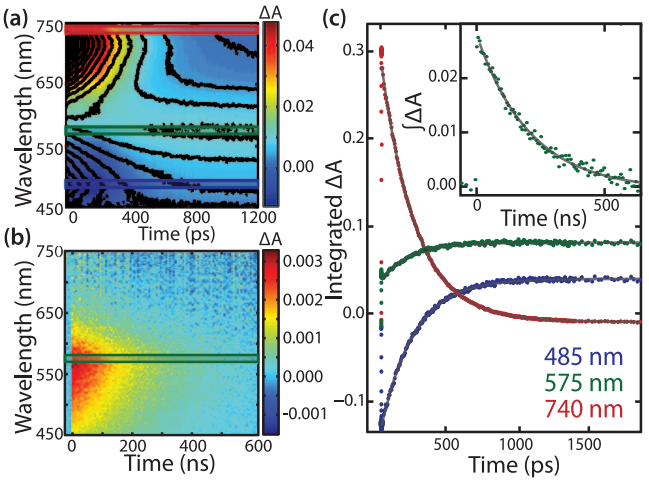

FIG. 5. Experimental characterization of electronic relaxation dynamics in BSC: (a) Ultrafast and (b) microsecond-regime transient absorption spectra. Outlined boxes show regions of interest integrated to quantify dynamics. (c) Results of integration of the regions of interest in the ultrafast transient absorption spectra, plotted along with fit results (black lines). The inset shows the results of integration of the lone region of interest in the microsecond-regime transient absorption spectra.

We present experimental characterization of relaxation dynamics after excitation at 395 nm in Fig. 5. Ultrafast transient absorption spectra (Fig. 5(a)) initially show a broad, negative feature at short wavelengths and a broad, positive feature at long wavelengths. The amplitude of these features decays with increasing time delay. A third broad feature, with positive amplitude centered near 575 nm, appears during the first nanosecond. A similar feature is present at the earliest times in the microsecond-regime transient absorption spectra (Fig. 5(b)), with initially positive amplitude decaying to zero over several hundred nanoseconds. To quantify the observed dynamics, we selected four regions of interest within the spectra. We chose three 10 nm wide regions in the ultrafast spectra to represent the short wavelength, negative feature (485 nm, blue), the long wavelength, positive feature (740 nm, black), and the feature that appears during the first nanosecond (575 nm, green), respectively. One region was chosen to represent the lone microsecond-regime absorption feature (575 nm, green). We integrate the signal at each time-delay within each region of interest, and fit the resulting data series to an appropriate exponential model (Fig. 5(c)) (see supplementary material).[69]

The 485 nm feature recovers from strongly negative initial amplitude toward a slightly positive long-time plateau with a single exponential time constant of 252.6 ps ± 1.2 ps (1 s.d.) The long-time positive plateau likely occurs because of overlap with the 575 nm feature. Integrating intensity from the blue edge (450-460 nm) of the negative feature and fitting to a single-exponential growth gives a timescale of 265 ps ± 10 ps. The data are noisier than the integrated signal at 485 nm due to low probe intensity, but also contains less interference from the 575 nm feature. This broad, negative feature results from a combination of ground state bleaching and stimulated emission.

The amplitude of the 740 nm feature decays from an initial positive value toward zero at long times, with a single exponential time constant of 266.2 ps ± 0.4 ps. We assign the 740 nm feature to excited state absorption by an exciton state. We find no early-time dynamics that can be assigned to exciton formation (see supplementary material),[69] indicating that the exciton is formed within our instrument response (~250 fs FWHM). The well-matched timescales for exciton decay and recovery of the negative amplitude feature support exciton recombination on a timescale of ~265 ps. We find the best correspondence between the well-resolved exciton feature at 740 nm and the bluest edge of the bleach feature, likely because the bluest edge of the feature contains the strongest bleaching contribution. The timescale for exciton recombination is also similar to the 276.5 ps ± 0.2 ps lifetime of the neutral excited state of BSC measured via time-correlated single photon counting (TCSPC),[69] indicating that exciton recombination may be radiative.

The 575 nm feature appears during the instrument response (see supplementary material),[69] then exhibits continued, slow growth during the next nanosecond. This slow growth displays a single exponential time constant of 227 ps ± 4 ps. The feature begins to decay within the first few nanoseconds. In the microsecond-regime transient absorption spectra, the lone broad positive feature decays with a time constant of 194 ns ± 7 ns. Both 575 nm features are consistent with a BSC cation state, although they may also be due to formation of a triplet excited state. We observe a BSC cation state in cation titration difference spectra, supporting assignment to cation formation.[69] Because these experiments are carried out in dilute solutions, BSC cation formation would eject electrons into the surrounding solvent, although the current data do not provide a direct probe of this process. Decay of the feature in the microsecond-regime spectra is due to either charge recombination or recombination of a triplet excited state.

The undecorated polymer (PLMR)

In this section, we present results characterizing electronic relaxation dynamics in a representative analogue of the alternating copolymer backbone of the DCP macromolecule, PLMR, in dilute THF solution. The linear absorption and fluorescence emission spectra of PLMR are presented in Fig. 6, along with the B3LYP-optimized structure of a representative tetramer. The absorption spectrum of PLMR shows a broad feature at 515 nm, with a small shoulder on the blue edge of the feature and a sharper red edge. The fluorescence emission spectrum has a sharp peak at 552 nm, a shoulder at 600 nm, and a broad, low-frequency tail extending out to ~750 nm. The dual-featured emission spectrum likely arises from a vibronic progression. The B3LYP-optimized structure of PLMR exhibits out-of-plane distortion around the thiophene groups in the copolymer backbone similar to that seen in BSC. Excited state calculations based on this structure predict the lowest energy optical transitions to be the strongest (TDDFT yields f = 4.6650, ZINDO yields f = 3.9545, respectively), and we assign the 522 nm absorption feature to this transition. The calculations predict that the transition will primarily consist of the HOMO to LUMO transition (TDDFT 48%,

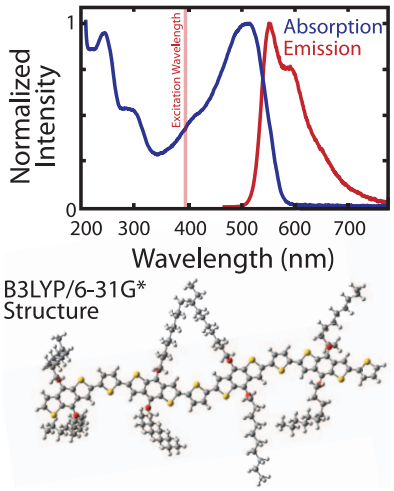

FIG. 6. Absorption and emission spectra of PLMR and optimized molecular structure: (Top) absorption (blue) and fluorescence emission (red, 394 nm excitation) spectra for PLMR. (Bottom) B3LYP-optimized structure of a PLMR-analogue. Atoms are color coded (white = H, grey = C, red = O, yellow = S).

ZINDO 53%). Our calculations indicate that for the HOMO to LUMO transition, electron density migrates toward the center of the polymer fragment and acquires significant nodal character, typical of a π–π^* transition in copolymer systems (see supplementary material).[69,72,78] Similar to the predicted important MO transitions in BSC, the HOMO to LUMO transition in PLMR also involves rearrangement of the double-bond structure from aromatic to quinoidal form.[69,79]

Experimental characterization of relaxation dynamics subsequent to excitation of PLMR at 395 nm is presented in Fig. 7. We chose to pump at 395 nm for consistency with BSC and DCP measurements. Experiments performed with 515 nm pump pulses yield similar results (see supplementary material).[69] We assign the spectra and dynamics in terms

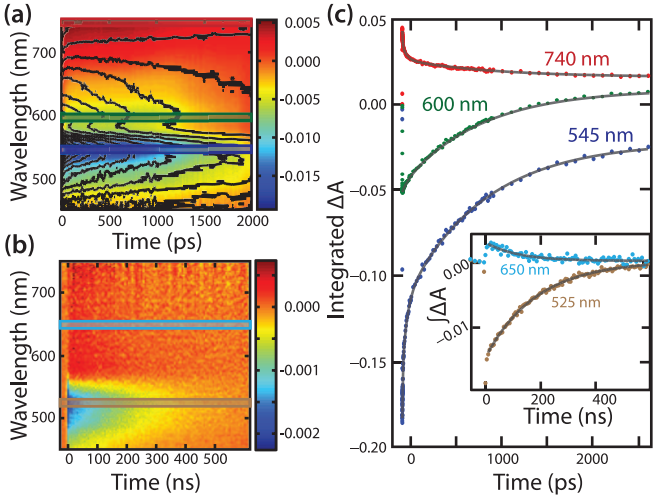

FIG. 7. Experimental characterization of PLMR relaxation dynamics: (a) Ultrafast and (b) microsecond-regime transient absorption spectra. Outlined boxes show regions of interest integrated to quantify dynamics. (c) Results of integration of the regions of interest in the transient absorption spectra, plotted along with fit results (black lines). The inset shows the results of integration of regions of interest in the microsecond regime transient absorption spectra.

of the frontier states of PLMR. Higher-lying excited states formed by absorption of 395 nm photons relax quickly into frontier state populations in accordance to Kasha's rule.[80] The lack of early-time dynamics that could be assigned to relaxation into S1 from higher lying excited states,[69] along with correspondence between dynamics measured at both 395 nm and 515 nm pump wavelengths, indicates very fast (<250 fs) relaxation into S1 from initially excited, higher-lying states that exhibit no absorption features in the spectral range considered here.

The ultrafast transient absorption spectra (Fig. 7(a)) contain a strong negative feature centered near 545 nm, a less strong negative feature at 600 nm, and a broad positive feature at wavelengths greater than ~700 nm. During the first few nanoseconds, the long wavelength feature decays toward a non-zero positive plateau. The 600 nm feature recovers intensity, eventually reaching a positive long time-delay plateau. The more intense negative feature at 545 nm recovers amplitude toward a nonzero negative plateau at long time-delays. In the microsecond-regime (Fig. 7(b)) spectra, two features are present: a broad, positive feature at long wavelengths, and a stronger negative feature centered near 525 nm. Both features decay toward zero amplitude as time-delay increases. No clearly resolved new features arise as time-delay increases in either the ultrafast or microsecond-regime spectra. The negative feature at 600 nm is not present in the long-delay spectra, and the positive-intensity, long-wavelength feature extends into this region. To quantify the observed dynamics, we chose five regions of interest in the transient absorption spectra. We chose three 10 nm wide regions in ultrafast transient absorption spectra to represent the strong negative feature (545 nm, blue), the weaker negative feature (600 nm, green), and the positive feature (740 nm, red). In the microsecond-regime spectra, we chose two regions to represent the broad negative (525 nm, tan) and positive (650 nm, cyan) features. We integrate the signal at each time-delay within each region of interest, and fit the resulting data series to an appropriate exponential model (Fig. 7(c)) (see supplementary material).[69]

The 545 nm feature has strong negative initial amplitude, and recovers toward zero with increasing time delay. The recovery is best fit by a triple exponential growth model, yielding time constants 5.5 ps ± 0.5 ps, 52 ps ± 4 ps, and 863 ps ± 26 ps. We assign this feature to a combination of ground state bleaching and stimulated emission. The center of the intense bleach feature blue-shifts by ~15 nm over the first few picoseconds, from ~545 nm to ~530 nm. This ~65 meV energy shift may be related to overlap with stimulated emission from the nearby fluorescent state shown in Fig. 6. The 545 nm feature decays to a nonzero plateau at long delay-times. The 525 nm feature in the microsecond-regime transient absorption spectra is assigned to slightly blue-shifted ground state bleaching, and recovers to zero amplitude with a single exponential time constant of 179 ns ± 3 ns.

The 740 nm feature has positive initial amplitude and decays toward a positive plateau at long time-delays. This decay is best fit by a triple exponential decay model, yielding time constants 4.3 ps ± 0.4 ps, 47 ps ± 6 ps, and 970 ps ± 101 ps. We assign this feature to transient excited state absorption by an exciton state.

The 600 nm feature has a negative initial amplitude and increases toward a slightly positive plateau at long time-delays. The increasing signal is best fit to a double exponential growth model, yielding time constants 52 ps ± 10 ps and 838 ps ± 17 ps. This feature is assigned as stimulated emission from the initially excite state, contaminated by interference from growth of the positive amplitude feature shown in the microsecond regime transient absorption spectra (Fig. 7(b)). The lack of the fastest of the three time constants observed in the 545 nm bleach feature may result from coincidental cancellation due to overlapping interference from the 740 nm and 545 nm features.

Microsecond-regime transient absorption spectra show positive intensity for wavelengths greater than ∼590 nm. The dynamics of this extremely broad feature are illustrated by the integrated signal around 650 nm, decaying from positive amplitude toward zero with a single exponential time constant of 118 ns ± 15 ns. Decay and recovery timescales on the order of a few hundred nanoseconds may indicate contributions from a long-lived triplet or trap state.

The similarity in timescales for exciton decay and ground state bleach recovery suggest tri-exponential exciton recombination, although triplet quenching pathways may also be present and the long lived features observed in the microsecond spectra are likely due to triplets formed during this process. The yield of the triplet-forming interstate crossing process cannot be determined from the present data, and we cannot definitively assign one of the relaxation timescales to triplet formation. The timescales for excited state absorption by the exciton most accurately represent the exciton recombination dynamics, because they are the least likely to be contaminated by overlap with other spectral features. The earliest dynamics, on the order of several picoseconds, are consistent with primary geminate recombination of tightly bound excitons in other OPV polymers in solution.[4,81] The middle relaxation time constant, ∼50 ps, is too long for primary geminate recombination but too short to be a radiative lifetime. The current data do not support more detailed assignment of this feature, although triplet quenching may be responsible. The longest recovered recombination timescales in PLMR correlate well with the measured 901.5 ps ± 0.6 ps excited state lifetime of PLMR, measured by TCSPC (see supplementary material),[69] and we assign those dynamics to radiative exciton recombination.

The decorated polymer

In this section, we present results characterizing electronic dynamics in the macromolecule DCP, in dilute THF solution. We apply computational results to assign localization of excitation in the absorption bands of DCP. We use transient absorption spectroscopy to characterize relaxation dynamics subsequent to initial excitation at 395 nm pump wavelength.

The absorption and fluorescence emission spectra of DCP are presented in Fig. 8, along the B3LYP-optimized structure and selected MOs from excited state calculations that illustrate excitation localization in DCP. The absorption spectrum of DCP shows a strong transition centered at 392 nm, a smaller, broader feature peaking at 513 nm, and a shoulder extending out to ∼600 nm. The DCP emission spectrum contains a single, broad peak centered at 599 nm and is independent of the excitation frequency (see supplementary material).[69] We optimized the geometry of a representative DCP-analogue at the B3LYP/6-31G* level. The molecule exhibits out-of-plane twisting through the polymer backbone and pendant side chains, similar to PLMR and BSC. The side chain groups tilt toward the polymer backbone in vacuum, such that one arm stacks approximately parallel to the polymer backbone. The preferred side chain geometry in solution phase DCP may be different than the gas-phase side chain arrangement in the calculated structure of the analog molecule. The branched side chains are free to rotate about the linking structure, and the full alkyl side chains on the BDT units in DCP molecule may inhibit the alignment shown in Fig. 8. Detailed computational determination of the preferred side chain orientation in full DCP and the energetic of side chains rotation about the linker required impractical computation times.

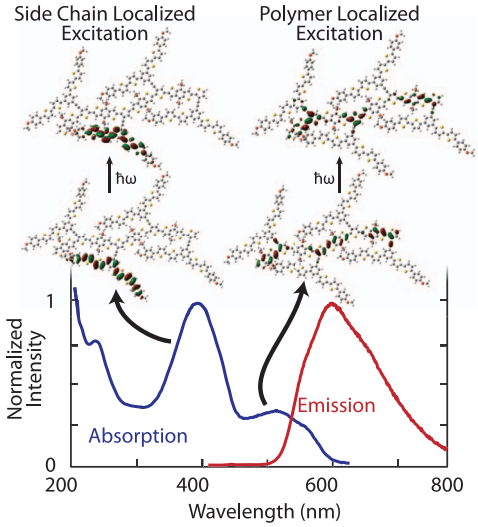

FIG. 8. Absorption and emission spectra of DCP and important molecular orbitals: Absorption (blue) and fluorescence emission (red, 394 nm excitation) spectra for DCP, and the B3LYP-optimized structure of a DCP-analogue. Examples of side chain localized (top left) and "polymer-like" (top right) MO-to-MO transitions contributing to the absorption spectrum, as calculated by TDDFT. Atoms are color coded (white = H, grey = C, red = O, yellow = S).

We characterize the low lying optical transitions of the DCP-analog molecule using TDDFT/6-31G* and ZINDO calculations. Both methods predict a strong lowest lying optical transition (λ = 438.7 nm and f = 2.9295 for TDDFT, λ = 581.0 nm and f = 2.5087 for ZINDO). Qualitative inspection reveals that the MOs contributing to this transition are strongly polymer localized, although TDDFT calculations show small amounts of mixing. The ZINDO/S calculation predicts that the most substantial contribution to this transition comes from a MO-to-MO transition that is very similar to the HOMO-to-LUMO transition of PLMR (see supplementary material).[69] Based on these results, we assign the lower energy absorption feature of DCP to a polymer-localized excitation.

Both computational methods predict a substantial gap between the polymer-localized excitation and the next-lowest

lying strong transition. TDDFT predicts a group of four closely spaced strong transitions at $\lambda = 361.8$ nm, 360.4 nm, 358.3 nm, and 352.2 nm, with oscillator strengths of $f = 2.4946$, 4.6780, 2.1727, and 4.2384, respectively. TDDFT predicts no other strong transitions above 275 nm. Qualitative inspection of the MOs contributing to these four excitations reveals that the three lower lying states are primarily localized on the side chain moieties, and while the fourth state is delocalized across both side chains and the polymer backbone. Some MO-to-MO transitions are localized on a single side chain, as shown in Fig. 8, while others have substantial amplitude on multiple side chains. ZINDO predicts a similar group of four states at $\lambda = 476.2$ nm, 472.6 nm, 469.7 nm, and 461.4 nm, with oscillator strengths $f = 1.5062$, 5.9523, 1.4520, and 3.7436, respectively. ZINDO calculations also predict no other strong optical transitions above 370 nm, and again predict side chain localized excitation for the three lower lying states in this group and mixed character for the fourth state. All MO-to-MO transitions predicted by both methods involve rearrangement of the double-bond structure from aromatic to quinoidal form (see supplementary material).[69,79] Based on these results, we assign the strong 395 nm absorption feature of DCP to a strongly side chain localized excitation. The observed localization confirms our design objective: weak electronic coupling between the polymer and side chain moieties in DCP. Meta-substitution of the central benzene ring core of the side chain moiety strongly decouples the side chain and polymer regions of the molecule, allowing each part to act as an independent chromophore. Although the lineshape of the DCP absorption spectrum resembles the "camel-back" structure commonly seen in alternating co-oligomers and copolymers, in which the redder peak is a charge transfer band and the bluer peak is a π–π^* transition,[69,78,79] our calculations do not predict strong charge transfer character for either absorption feature.

Fig. 9 presents experimental characterization of relaxation dynamics subsequent to excitation of DCP at 395 nm. The ultrafast spectra (Fig. 9(a)) contain a positive feature extending from 600 nm to 750 nm, and a negative feature in the 450-600 nm region. The positive feature appears to contain two components, centered at 630 nm and 740 nm, respectively. The negative feature also appears to contain two components, at 525 nm and 565 nm. The amplitude of all features decays sharply in the sub-picosecond regime (see supplementary material),[69] followed by further decay over longer timescales. Dynamics subsequent to pumping at 515 nm were also measured,[69] yielding dynamics similar to those presented in Fig. 9 but lacking the ultrafast relaxation component. To quantify the observed dynamics, we selected five regions of interest within the spectra. We chose three 10 nm wide regions in the ultrafast spectra to represent the longer (740 nm, red) or shorter (630 nm, green) wavelength positive features, and a single region to represent the broad negative feature (525 nm, blue). Visual inspection of the transient absorption spectra suggests that a fourth component at 565 nm should be analyzed, but dynamics in that region are indistinguishable from those at 525 nm and are not discussed further. Two regions were chosen to represent the positive (650 nm, cyan) and negative (525 nm, tan) microsecond-regime absorption features.

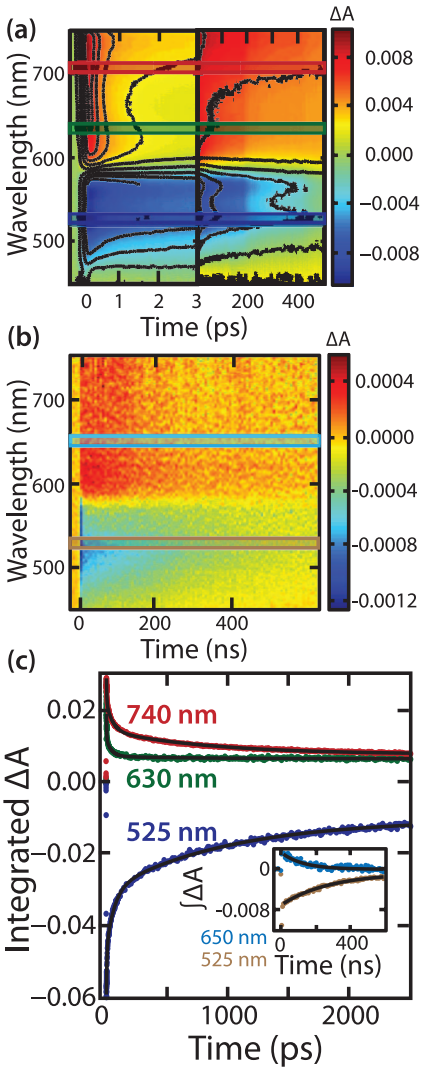

FIG. 9. Experimental characterization of DCP relaxation dynamics: (a) Ultrafast and (b) microsecond-regime transient absorption spectra. Outlined boxes show regions of interest integrated to quantify dynamics. (c) Results of integration of the regions of interest in the transient absorption spectra, plotted along with fit results (red lines.) The inset shows the results of integration of regions of interest in the microsecond regime transient absorption spectra.

We integrated the signal at each time-delay within each region of interest, and fit the resulting data series to an appropriate exponential model (Fig. 9(c)).

We assign the broad negative feature to a combination of ground state bleaching and stimulated emission. The feature shows strong sub-picosecond dynamics (see supplementary material),[69] recovering >50% amplitude during the first 2.5 ps. Further recovery, toward a slightly negative plateau at long delay-times, fits well to a triple exponential growth model (Fig. 9(c)), yielding time constants 5.7 ps ± 0.4 ps, 68 ps ± 2 ps, and 988 ps ± 24 ps. These dynamics are consistent across most of the broad feature, although at the reddest edge of the feature, around 580 nm, the fastest component disappears, along with the sub-picosecond dynamics.

We assign the broad, positive feature at 740 nm to transient absorption by an exciton state. The feature has strong initial positive amplitude, and decays by ∼50% in the

subpicosecond regime (see supplementary material).[69] Further decay, toward slight positive plateau at long time-delays, is well fit by a triple exponential decay model, yielding decay time constants 5.6 ps ± 0.2 ps, 61 ps ± 2 ps, and 902 ps ± 22 ps.

The similarity in the picosecond-scale time constants for recovery of the negative feature and exciton decay indicates multi-component intramolecular exciton recombination. Triplet formation may also contribute. The similarity between the longest observed recombination timescale and the excited state lifetime measured by TCSPC, 1126 ps ± 2 ps (see supplementary material),[69] suggests that this slowest process is radiative despite slight disagreement in fitted lifetimes. The fastest exponential timescale recovered, ∼5 ps, is consistent with primary geminate exciton recombination, similar to that seen in PLMR sub-picosecond relaxation dynamics[69] may be due to exciton diffusion followed by exciton-exciton annihilation, or to ultrafast intramolecular exciton dissociation. Control experiments performed with varying pump powers suggest that this fast component varies quadratically with laser fluence supporting our assignment of this feature to exciton-exciton annihilation.[69] Corresponding dynamics in both the exciton and bleach/stimulated-emission features indicate that exciton-exciton annihilation is present, though this evidence does not rule out that ultrafast intramolecular exciton dissociation is also occurring and quenching of the singlet excited state due to triplet formation is also consistent with this pattern.

At 630 nm, sub-picosecond dynamics are similar to the 740 nm feature (see supplementary material).[69] Relaxation dynamics at 630 nm fits best to a double exponential decay model, yielding time constants of 2.4 ps ± 0.4 ps and 45 ps ± 4 ps. Comparing these dynamics to those of the 740 nm feature, we find slightly faster early time constants and no radiative recombination component. The timescales measured here are consistent with previous dynamics assigned to decay of a charge separated state in conjugated polymers similar to PLMR,[4] but the current data do not support a detailed analysis of charge-separation in DCP because we lack a direct spectral signature of the cation state of PLMR. Further experiments, including transient absorption with the near infrared detection, are required to understand how charge separated states behave in DCP. For this work, we restrict our discussion to exciton decay and migration rather because we recovered no clear spectral signatures of charge-separated states.

In the microsecond-regime transient absorption experiments (Fig. 9(c)), broad negative and positive features, appearing at shorter and longer wavelengths, decay to zero amplitude with time constants of 279 ns ± 13 ns and 113 ns ± 13 ns, respectively. Relaxation dynamics are indistinguishable across the full breadth of both features. Relaxation dynamics on the order of 100 ns, similar to the dynamics observed PLMR, suggest a trap or triplet state.

Localized excitation in DCP

In designing DCP, we employ meta-substitution around the benzene ring comprising the side chain core to break conjugation between the side chain branches and the polymer, enforcing weak electronic coupling between the constituent moieties of DCP. This strategy is intended to ensure that excitations can be considered as either side chain-localized or polymer-localized (see supplementary material).[69]

Comparison of the normalized absorption spectra of BSC, PLMR, and DCP (see supplementary material)[69] demonstrates striking qualitative correspondence between the spectral position and lineshape of the two major features in the absorption spectrum of DCP and the major features in the BSC and PLMR absorption spectra.[69] The 392 nm feature in the DCP absorption spectrum is very similar to the 394 nm feature in the BSC absorption spectrum, with the DCP feature being slightly broader, especially on the red edge. The 513 nm feature in the DCP spectrum is similar to the 515 nm feature in the PLMR spectrum, again with the DCP feature being broader on the red edge. Correspondence in spectral positions are consistent with, but not unilaterally indicative of, a low-electronic-coupling regime, with the 392 nm feature assigned to slightly blue-shifted, side chain localized absorption and the 513 nm feature assigned to polymer localized excitation.

Excited state calculations predict the optical transitions to the low-lying excited states of DCP and support the localized excitation model. Both density functional and semi-empirical calculations predict that the lowest-lying electronic transition is strong and localized on the polymer. Both calculations also predict a group of higher lying strong transitions localized on the side chains. These results support assignment of the 513 nm and 392 nm absorption features of DCP to polymer and side chain localized transitions, respectively.

Engineering energy flow in DCP

We employ two important design strategies in the synthesis of DCP that make it a model system for demonstrating energy transfer from optically active pendant side chains into the polymer backbone. As discussed in the section on Localized excitation in DCP, we employ a meta-substitution strategy at the core of our branched side chain that enforces weak coupling between the optically active parts of the molecule. Weak coupling ensures that the constituent parts of the molecule are independent chromophores, and energy transfer between them can occur in a meaningful way. In a more strongly coupled system, excitations would be substantially delocalized over both the conjugated backbone and side chain components simultaneously. Energy transfer between the two moieties would be poorly defined. To maximize energy transfer between the side chains and the polymer, we select the side chain and polymer components to maximize overlap between the emission spectrum of BSC and the absorption spectrum of PLMR. We also use short linkers, relative to previous studies of energy transfer in conjugated polymers coupled to absorbers.[49–52] Our rigid linking structure also creates a well-defined spatial relationship between the chromophores, although the degree to which side chains rotate about the linking structure has not been determined due to the size of the system. A longer, more flexible linker, such as those employed in previous studies of energy transfer between conjugated polymers and optically active side chains,[49,50] creates a wide

variety of interchromophore distances and orientations within any experimentally measured ensemble. This inhomogeneity obscures detailed analysis of the energy transfer dynamics.

Our results support ultrafast transfer of initially side chain localized excitations to the polymer part of DCP within our experimental instrument response (250 fs FWHM). As described above, computational results and comparison with spectra of control materials indicate that excitation at 395 nm is primarily side chain localized. Several pieces of evidence demonstrate that this excitation is transferred to the polymer within 250 fs. First, relaxation dynamics following 395 nm excitation of PLMR and DCP strongly agree, for time delays beyond the first few picoseconds. Relaxation dynamics following 515 nm excitation also show a similar correspondence (see supplementary material).[69] Although the time constants for three-component relaxation in each case do not agree within one standard deviation error, they do correspond generally, and show striking contrast with electronic relaxation dynamics in BSC (Fig. 6). Second, transient absorption experiments performed on a mixture of unlinked BSC and PLMR in THF solution, with the ratio of solution components set to mimic the absorption spectrum of DCP, produce distinctly BSC-like spectra and dynamics.[69] This result indicates that the close spatial proximity established via the rigid alkynyl linkers in DCP is required to establish energy transfer between the side chain and polymer moieties. Finally, fluorescence excitation and emission spectra and excited state lifetimes in DCP and PLMR are very similar, regardless of whether DCP is pumped at 395 nm or 515 nm.[69] This similarity strongly supports energy transfer from the sidechain to the backbone. DCP fluorescence emission spectra and fluorescence lifetime are very different from the fluorescence parameters of BSC. This comparison indicates that initially side chain localized excitations become polymer localized prior to fluorescence emission.

Taken together, these results generate a picture in which side chain localized excitation of DCP at 395 nm leads to ultrafast energy transfer into a polymer localized state. Once the initial excitation is transferred, exciton recombination proceeds through the same mechanisms seen in PLMR. A kinetic scheme of this energy transfer and relaxation picture is shown in Fig. 10. Competing formation of a DCP cation may also be present, but lacking strong evidence we leave this factor out of the current analysis.

To date, ultrafast energy transfer dynamics between a conjugated polymer and optically active side chains have only been quantified in one previous study,[49] demonstrating energy transfer from a conjugated polyfluorene into optically active Ru(II)-based side chains in ∼500 fs. Side chains in the previous study were attached by long, flexible linkers, and the shorter interchromophore distance in our DCP molecule likely accounts for the faster energy transfer. Hydrogen-bound moieties[51] and macrocycle side chains[52] have been explored as light-harvesting antennae coupled to conjugated homopolymers. However, the combination of light-harvesting side chains and high performance alternating copolymers is relatively unexplored.

While the rigid nature of the linker is unlikely to play a role in determining the rate of energy transfer, this property may enable DCP to support interesting coherent electronic behavior. Energy transfer dynamics[57] and energy transfer quantum yield[54–56,58] have been studied in detail in a number of rigidly linked systems using dendrimers as energy donors and conjugated small molecules as acceptors. The quantum yield of energy transfer in rigid, linked donor-acceptor macromolecules can be strongly enhanced through coherence control experiments, demonstrating that coherent effects can play a role in energy transfer in these systems.[53] The rigid nature of DCP may support similar behavior, although the current experimental results do not permit further comment.

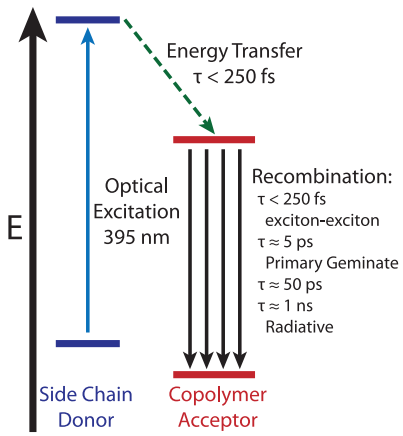

FIG. 10. Kinetic scheme for DCP: A kinetic scheme for relaxation in DCP, subsequent to excitation at 395 nm. Ultrafast energy transfer from an initially side chain localized excited state into a polymer localized state is followed by multi-stage exciton recombination. In the through space energy transfer mechanism considered here, energy transfer leaves the side chain donor in its neutral ground state and both excited electron and a hole move to the copolymer.

CONCLUSION

In this study, we use solution phase, time resolved spectroscopy to demonstrate ultrafast energy transfer between the weakly coupled constituent parts of a macromolecule in which we couple singly branched, rigidly linked, optically active pendant side chains to a conjugated, alternating copolymer. This result shows that excitation migration in macromolecular systems with multiple optically active components can be controlled through molecular design. The short, rigid linking strategy that we employ facilitates fast energy transfer while maintaining a well-defined spatial relationship between side chains and polymer. In future materials based on this design concept, the singly branched side chains we employ may support either further branching into dendrimers or attachment of a third optically active component.

ACKNOWLEDGMENTS

This research was supported by the DARPA QuBE program (Grant No. N66001-10-1-4060) and National Science Foundation (NSF) MRSEC (Grant No. DMR 08-02054). We thank Dr. Matthew Pelton for assistance with transient absorption experiments and helpful discussions. We thank Dr.

Zbigniew Gasyna for help carrying out our computational studies. We thank Dr. Justin Jurreler for help with fluorescence and TCSPC measurements. Use of the Center for Nanoscale Materials was supported by the (U.S.) Department of Energy (DOE), Office of Science, Office of Basic Energy Sciences, under Contract No. DE-AC02-06CH11357. We acknowledge contributions to this work from the Institute for Biophysical Dynamics NanoBiology Facility and National Institutes of Health (NIH) Grant No. 1S10RR026988-01.

[1]T. M. Clarke and J. R. Durrant, Chem. Rev. (Washington, DC) **110**, 6736 (2010).
[2]D. C. Coffey, A. J. Ferguson, N. Kopidakis, and G. Rumbles, ACS Nano **4**, 5437 (2010).
[3]X.-Y. Zhu, Q. Yang, and M. Muntwiler, Acc. Chem. Res. **42**, 1779 (2009).
[4]B. S. Rolczynski, J. M. Szarko, H. J. Son, Y. Y. Liang, L. P. Yu, and L. X. Chen, J. Am. Chem. Soc. **134**, 4142 (2012).
[5]N. Banerji, J. Mater. Chem. C **1**, 3052 (2013).
[6]B. Kraabel, C. H. Lee, D. McBranch, D. Moses, N. S. Sariciftci, and A. J. Heeger, Chem. Phys. Lett. **213**, 389 (1993).
[7]C. J. Brabec, G. Zerza, G. Cerullo, S. De Silvestri, S. Luzzati, J. C. Hummelen, and S. Sariciftci, Chem. Phys. Lett. **340**, 232 (2001).
[8]L. G. Kaake, G. C. Welch, D. Moses, G. C. Bazan, and A. J. Heeger, J. Phys. Chem. Lett. **3**, 1253 (2012).
[9]A. A. Paraecattil, S. Beaupre, M. Leclerc, J.-E. Moser, and N. Banerji, J. Phys. Chem. Lett. **3**, 2952 (2012).
[10]I. Hwang, S. Beaupre, M. Leclerc, and G. D. Scholes, Chem. Sci. **3**, 2270 (2012).
[11]A. A. Bakulin, A. Rao, V. G. Pavelyev, P. H. M. van Loosdrecht, M. S. Pshenichnikov, D. Niedzialek, J. Cornil, D. Beljonne, and R. H. Friend, Science **335**, 1340 (2012).
[12]M. J. Bedard-Hearn, F. Sterpone, and P. J. Rossky, J. Phys. Chem. A **114**, 7661 (2010).
[13]M. A. Stevens, C. Silva, D. M. Russell, and R. H. Friend, Phys. Rev. B **63**, 165213 (2001).
[14]R. Tautz, E. Da Como, T. Limmer, J. Feldmann, H.-J. Egelhaaf, E. von Hauff, V. Lemaur, D. Beljonne, S. Yilmaz, I. Dumsch, S. Allard, and U. Scherf, Nature Commun. **3**, 970 (2012).
[15]J. Piris, T. E. Dykstra, A. A. Bakulin, P. H. M. van Loosdrecht, W. Knulst, M. T. Trinh, J. M. Schins, and L. D. A. Siebbeles, J. Phys. Chem. C **113**, 14500 (2009).
[16]O. G. Reid, J. A. N. Malik, G. Latini, S. Dayal, N. Kopidakis, C. Silva, N. Stingelin, and G. Rumbles, J. Polym. Sci., Part B: Polym. Phys. **50**, 27 (2012).
[17]M. Scarongella, A. Laktionov, U. Rothlisberger, and N. Banerji, J. Mater. Chem. C **1**, 2308 (2013).
[18]S. B. Darling and F. You, RSC Adv. **3**, 17633 (2013).
[19]L. S. C. Pingree, B. A. MacLeod, and D. S. Ginger, J. Phys. Chem. C **112**, 7922 (2008).
[20]A. P. Kulkarni, X. Kong, and S. A. Jenekhe, Macromolecules **39**, 8699 (2006).
[21]C.-H. Tsai, K.-C. Tien, M.-C. Chen, K.-M. Chang, M.-S. Lin, H.-C. Cheng, Y.-H. Lin, H.-W. Chang, H.-W. Lin, C.-L. Lin, and C.-C. Wu, Org. Electron. **11**, 439 (2010).
[22]D. R. Mccamey, K. J. Van Schooten, W. J. Baker, S.-Y. Lee, S.-Y. Paik, J. M. Lupton, and C. Boehme, Phys. Rev. Lett. **104**, 017601 (2010).
[23]J. M. Lupton, D. R. Mccamey, and C. Boehme, Chem. Phys. Chem. **11**, 3040 (2010).
[24]L. A. Estrada, V. A. Montes, G. Zyryanov, and J. P. Anzenbacher, J. Phys. Chem. B **111**, 6983 (2007).
[25]L. Shang, M. Liu, D. Tu, L. Zhen, G. Liu, R. Jia, L. Li, and W. Hu, Thin Solid Films **516**, 5093 (2008).
[26]H. N. Tsao, D. Cho, J. W. Andreasen, A. Rouhanipour, D. W. Breiby, W. Pisula, and K. Müllen, Adv. Mater. (Weinheim) **21**, 209 (2009).
[27]M. M. Payne, S. R. Parkin, J. E. Anthony, C.-C. Kuo, and T. N. Jackson, J. Am. Chem. Soc. **127**, 4986 (2005).
[28]F. Silvestri, A. Marrocchi, M. Seri, C. Kim, T. J. Marks, A. Facchetti, and A. Taticchi, J. Am. Chem. Soc. **132**, 6108 (2010).
[29]J. Lehmann, A. Gaita-Ariño, E. Coronado, and D. Loss, J. Mater. Chem. **19**, 1672 (2009).
[30]D. Beljonne, Z. Shuai, G. Pourtois, and J. L. Bredas, J. Phys. Chem. A **105**, 3899 (2001).
[31]Y. Liang, Z. Xu, J. Xia, S.-T. Tsai, Y. Wu, G. Li, C. Ray, and L. Yu, Adv. Mater. (Weinheim) **22**, E135 (2010).
[32]G. Li, R. Zhu, and Y. Yang, Nature Photon. **6**, 153 (2012).
[33]G. Dennler, M. C. Scharber, and C. J. Brabec, Adv. Mater. (Weinheim) **21**, 1323 (2009).
[34]C. W. Tang, Appl. Phys. Lett. **48**, 183 (1986).
[35]J. You, L. Dou, K. Yoshimura, T. Kato, K. Ohya, T. Moriarty, K. Emery, C.-C. Chen, J. Gao, G. Li, and Y. Yang, Nature Commun. **4**, 1446 (2013).
[36]D. Mühlbacher, M. Scharber, M. Morana, Z. Zhu, D. Waller, R. Gaudiana, and C. Brabec, Adv. Mater. (Weinheim) **18**, 2884 (2006).
[37]Y.-J. Cheng, S.-H. Yang, and C.-S. Hsu, Chem. Rev. (Washington, DC) **109**, 5868 (2009).
[38]S. Loser, C. J. Bruns, H. Miyauchi, R. O. P. Ortiz, A. Facchetti, S. I. Stupp, and T. J. Marks, J. Am. Chem. Soc. **133**, 8142 (2011).
[39]L. Blankenburg, K. Schultheis, H. Schache, S. Sensfuss, and M. Schrödner, Solar Energy Mater. Solar Cells **93**, 476 (2009).
[40]Y. Liang, S. Xiao, D. Feng, and L. Yu, J. Phys. Chem. C **112**, 7866 (2008).
[41]Y. Liang, D. Feng, Y. Wu, S.-T. Tsai, G. Li, C. Ray, and L. Yu, J. Am. Chem. Soc. **131**, 7792 (2009).
[42]D. J. Lipomi, B. C. K. Tee, M. Vosgueritchian, and Z. Bao, Adv. Mater. (Weinheim) **23**, 1771 (2011).
[43]B. E. Hardin, E. T. Hoke, P. B. Armstrong, J.-H. Yum, P. Comte, T. Torres, J. M. J. Frechet, M. K. Nazeeruddin, M. Gratzel, and M. D. McGehee, Nature Photon **3**, 406 (2009).
[44]Y. Liang, Y. Wu, D. Feng, S.-T. Tsai, H.-J. Son, G. Li, and L. Yu, J. Am. Chem. Soc. **131**, 56 (2009).
[45]Y. Liang and L. Yu, Acc. Chem. Res. **43**, 1227 (2010).
[46]H. J. Son, W. Wang, T. Xu, Y. Liang, Y. Wu, G. Li, and L. Yu, J. Am. Chem. Soc. **133**, 1885 (2011).
[47]N. Banerji, S. Cowan, M. Leclerc, E. Vauthey, and A. J. Heeger, J. Am. Chem. Soc. **132**, 17459 (2010).
[48]J. Mei, Y. Diao, A. L. Appleton, L. Fang, and Z. Bao, J. Am. Chem. Soc. **135**, 6724 (2013).
[49]L. Wang, E. Puodziukynaite, R. P. Vary, E. M. Grumstrup, R. M. Walczak, O. Y. Zolotarskaya, K. S. Schanze, J. R. Reynolds, and J. M. Papanikolas, J. Phys. Chem. Lett. **3**, 2453 (2012).
[50]H. Yeo, K. Tanaka, and Y. Chujo, Macromolecules **46**, 2599 (2013).
[51]S. A. Schmid, R. Abbel, A. P. H. J. Schenning, E. W. Meijer, and L. M. Herz, Philos. Trans. R. Soc. A **370**, 3787 (2012).
[52]K. Becker, P. G. Lagoudakis, G. Gaefke, S. Höger, and J. M. Lupton, Angew. Chem., Int. Ed. **46**, 3450 (2007).
[53]D. G. Kuroda, C. P. Singh, Z. Peng, and V. D. Kleiman, Science **326**, 263 (2009).
[54]D. W. Brousmiche, J. M. Serin, J. M. J. Fréchet, G. S. He, T.-C. Lin, S.-J. Chung, P. N. Prasad, R. Kannan, and L.-S. Tan, J. Phys. Chem. B **108**, 8592 (2004).
[55]O. Varnavski, I. D. W. Samuel, L. O. Palsson, R. Beavington, P. L. Burn, and T. Goodson, J. Chem. Phys. **116**, 8893 (2002).
[56]A. Adronov, S. L. Gilat, J. M. J. Fréchet, K. Ohta, F. V. R. Neuwahl, and G. R. Fleming, J. Am. Chem. Soc. **122**, 1175 (2000).
[57]E. Fron, L. Puhl, I. Oesterling, C. Li, K. Müllen, F. C. De Schryver, J. Hofkens, and T. Vosch, Chem. Phys. Chem. **12**, 595 (2011).
[58]A. Nantalaksakul, D. R. Reddy, C. J. Bardeen, and S. Thayumanavan, Photosynth. Res. **87**, 133 (2006).
[59]H. Frauenrath, Prog. Polym. Sci. **30**, 325 (2005).
[60]R. Jakubiak, Z. Bao, and L. J. Rothberg, Synth. Met. **116**, 41 (2001).
[61]R. Jakubiak, Z. Bao, and L. Rothberg, Synth. Met. **114**, 61 (2000).
[62]D. Marsitzky, R. Vestberg, P. Blainey, B. T. Tang, C. J. Hawker, and K. R. Carter, J. Am. Chem. Soc. **123**, 6965 (2001).
[63]C.-H. Chou and C.-F. Shu, Macromolecules **35**, 9673 (2002).
[64]T. Sato, D.-L. Jiang, and T. Aida, J. Am. Chem. Soc. **121**, 10658 (1999).
[65]A. Pogantsch, C. Gadermaier, G. Cerullo, G. Lanzani, U. Scherf, A. C. Grimsdale, K. Müllen, and E. J. W. List, Synth. Met. **139**, 847 (2003).
[66]J. Yu, K. H. Lee, Y. Zhang, M. F. G. Klein, A. Colsmann, U. Lemmer, P. L. Burn, S.-C. Lo, and P. Meredith, Polym. Chem. **2**, 2668 (2011).
[67]T. Kaneko, T. Horie, M. Asano, T. Aoki, and E. Oikawa, Macromolecules **30**, 3118 (1997).
[68]Q.-S. Hu, C. Sun, and C. E. Monaghan, Tetrahedron Lett. **43**, 927 (2002).
[69]See supplementary material at http://dx.doi.org/10.1063/1.4855156 for synthetic details, additional experimental data, and control experiments.

[70]R. C. Coffin, J. Peet, J. Rogers, and G. C. Bazan, Nature Chem. **1**, 657 (2009).
[71]M. J. Frisch, G. W. Trucks, H. B. Schlegel *et al.*, GAUSSIAN 09, Revision A.02, Gaussian, Inc., Wallingford, CT, 2009.
[72]C. Risko, M. D. Mcgehee, and J.-L. Brédas, Chem. Sci. **2**, 1200 (2011).
[73]A. D. Becke, J. Chem. Phys. **98**, 5648 (1993).
[74]R. Bauernschmitt and R. Ahlrichs, Chem. Phys. Lett. **256**, 454 (1996).
[75]J. Ridley and M. Zerner, Theor. Chim. Acta **32**, 111 (1973).
[76]A. Yokooji, T. Satoh, M. Miura, and M. Nomura, Tetrahedron **60**, 6757 (2004).
[77]D. Fichou, J. Mater. Chem. **10**, 571 (2000).
[78]J. M. Szarko, B. S. Rolczynski, J. Guo, Y. Liang, F. He, M. W. Mara, L. Yu, and L. X. Chen, J. Phys. Chem. B **114**, 14505 (2010).
[79]K. G. Jespersen, W. J. D. Beenken, Y. Zaushitsyn, A. Yartsev, M. Andersson, T. n. Pullerits, and V. Sundström, J. Chem. Phys. **121**, 12613 (2004).
[80]M. Kasha, H. R. Rawls, and M. A. El-Bayoumi, Pure Appl. Chem. **11**, 371 (1965).
[81]J. Guo, H. Ohkita, H. Benten, and S. Ito, J. Am. Chem. Soc. **131**, 16869 (2009).